Title

Validating compositional fluid flow simulations using 4D seismic interpretation and vice versa in the SECARB Early Test—A critical review

Authors
Alfi, Masoud
Vasco, Donald W
Hosseini, Seyyed A
et al.

Publication Date
2019-03-01

DOI
10.1016/j.ijggc.2019.01.003

Peer reviewed

Validating compositional fluid flow simulations using 4D seismic interpretation and vice versa in the SECARB Early Test—A critical review

Masoud Alfi[a], Donald W. Vasco[b], Seyyed A. Hosseini[c,*], Timothy A. Meckel[c], Susan D. Hovorka[c]

[a] Petroleum Engineering Department, Texas A&M University, College Station, TX

[b] Lawrence Berkeley National Laboratory, Berkeley, CA

[c] Bureau of Economic Geology, The University of Texas at Austin, Austin, TX

Abstract

This paper discusses strengths and weaknesses of 4D seismic interpretation as a technique for monitoring carbon dioxide that was injected as part of a large scale test associated with commercial enhanced oil recovery (EOR) at Cranfield Field, Mississippi, USA. The goals of the monitoring effort are 1) to make measurements to verify that the CO_2 is contained in the reservoir according to operational designs and model predictions, and 2) that if there are deviations, to provide data which can be used to update the earth models and determine if any mitigation is needed. The current work uses a compositional numerical simulation to model CO_2 flow in the reservoir and compares the results with estimates of changes in seismic properties between a pre-injection and a survey after more than 2 million metric tons injected. The complicated physics of the problem in Cranfield field present challenges to seismic interpretations. Our results show partial agreement between the results of the numerical simulation and the seismic interpretations. Possible causes of discrepancies among the fluid flow model and multiple interpretations of the same seismic data sets performed with different work flows illuminates the types of uncertainties that should be considered to achieve the goals of monitoring.

Keywords

[*] Future correspondences should be addressed to S. A. Hosseini (seyyed.hosseini@beg.utexas.edu)
University Station, Box X, Austin, Texas 78713-8924

CO_2 injection monitoring; 4D seismic; Compositional simulation; Enhanced oil recovery

1. Introduction

An important aspect of underground CO_2 injection, as an enhanced oil recovery method or as part of carbon capture and storage, is to monitor and track the movement of the carbon dioxide. This will help in maintaining a more effective sweep during EOR operation or improved effective storage during CO_2 sequestration. An increasing amount of time-lapse surface seismic work is being used for CO_2 injection monitoring. Arts et al. (2004) presented the results of seismic interpretations to monitor CO_2 injection into a saline aquifer at the Sleipner site. Their pioneering work was one of the first to use repeated time-lapse seismic surveys to monitor a large CO_2 injection and storage operation. Several subsequent seismic monitoring efforts have been conducted, such as those at the Weyburn (Davis et al., 2003), Otway (Urosevic et al., 2011), and Ketzin (Ivanova et al., 2012) reservoirs.

Alfi and Hosseini (2016) analyzed CO_2 injection into the Lower Tuscaloosa Formation of Cranfield field by comparing the results of a black oil numerical simulation of CO_2 movement with several seismic interpretations (Carter, 2014; Ditkof et al., 2011; Zhang et al., 2014). Their analyses showed that the flow simulation results and the seismic interpretations agree in some locations while diverging in others. In this paper, we will investigate the possible reasons for the observed discrepancies. Seismic technology provides a key advantage in monitoring CO_2 injection sites by covering a large acreage in a single survey. However, the application of 4D seismic for CO_2 plume tracking has always been hampered by several different factors (Gendrin et al., 2013; Ivanova et al., 2012; Roach et al., 2016). One challenge is the depth of the formation of interest. Generally, the deeper the reservoir, the harder it becomes to detect the induced changes in seismic signals because of CO_2 injection. Formation geology and rock properties, e.g. high rock stiffness, are additional factors that can negatively affect the reliability of seismic interpretations. The sensitivity of seismic surveys to changes in acoustic impedance make them highly sensitive in some, but not all geological contexts. Such effects can be magnified in environments with higher noise levels (e.g. onshore fields). Formation heterogeneity is another factor that influence our seismic interpretations. Regions with low porosity rocks, the presence of low-density layers (e.g.

coal) in the overburden, or non-homogeneous mixing of CO_2 with the formation fluid leading to the formation of patches, are examples of the effect of heterogeneity. Properties of the reservoir pore fluids prior to CO_2 injection and the presence of residual gas or a low-density oil phase in the reservoir provides another challenge for seismic monitoring of CO_2 injection, as will be discussed in more detail in the following sections. In addition, thickness of the accumulated carbon dioxide itself can impact the interpretation results. Thin plumes, below about one quarter of a wavelength, will not be detected in seismic survey.

Alfi and Hosseini (2016) modeled the CO_2 injection process using a black oil simulator (CMG-IMEX). Such an approach is effective specifically for large models with a significant number of grid blocks as it reduces the computational cost. On the other hand, black oil simulators come with the cost of not accurately modeling the miscibility of the CO_2 and reservoir fluids (oil and brine). Hence, in the current paper, we have improved the model by using a compositional simulator (CMG-GEM), which allows us to account for the CO_2 miscibility in oil and brine. Compositional models are better suited to deal with interaction between the various chemical components in the system, such as gas exsolution and dissolution. Accurate modeling of the distribution of gas is of a particular interest in this study and will be discussed in greater detail later in this paper.

In addition, in this study a new set of seismic interpretations were performed and compared to the interpretations by Carter (2014) and Ditkof et al. (2011) . Such a comparison helps us to understand how various processing and workflow choices impact seismic interpretations.

This paper begins with a descriptive explanation of the reservoir static and dynamic model. Oil, gas, and water production data are history matched and the model is tuned accordingly. Moreover, we explain how seismic data were prepared and interpreted. Seismic interpretations (from this paper and previous works) are then compared with dynamic simulation results, following a critical discussion on the role of different reservoir related factors on seismic data interpretation.

1. Numerical model description

In this study, we use data collected from the Cranfield site to history match fluid flow simulations. The Cranfield field is located in Adams and Franklin Counties, Mississippi, east of the town of Natchez. The original productive area of the reservoir was estimated to be 31.3 km^2 with a producing depth range of 3060 to 3193 m (Weaver and Anderson, 1966). An active aquifer downdip of the reservoir provides a constant pressure boundary. The initial reservoir temperature was reported to be 125°C with an initial reservoir pressure of 32.4 MPa at 3040 m. A central graben-bounding sealing fault, down dropped to the west, divides the productive zone into two reservoirs, and creates a trap on the east side (the dashed NW-SE line in Figure 1a). More details about reservoir specifications, production history, simulation projects, and monitoring efforts can be found in other publications (Alfi and Hosseini, 2016; Alfi et al., 2015; Choi et al., 2011; Hosseini et al., 2013; Hovorka et al., 2013; Weaver and Anderson, 1966). The current work focuses on the northeastern part of the reservoir, assuming a negligible fluid movement between this part and the rest of the reservoir, as the small contact area and balanced field development plan minimizes such flow. This approach has substantially decreased the number of active grid blocks in the system, in order to reduce the computational cost because compositional models increase the computational burden due the higher number of components in the system. A Cartesian model with 124 ×149×20 (X×Y×Z) grid cells is used to model a total reservoir area of 7.5 km by 9.1 km with a total reservoir thickness of 24.4 m. Total number of grid blocks is 369,520, out of which 82,559 grid blocks located at the northeastern part of the reservoir are considered to be active (Figure 1b). All grid blocks have a uniform dimension of 61×61×1.2 m. The simulation model is isothermal and does not account for the possible reactions between minerals, injected and in situ fluids.

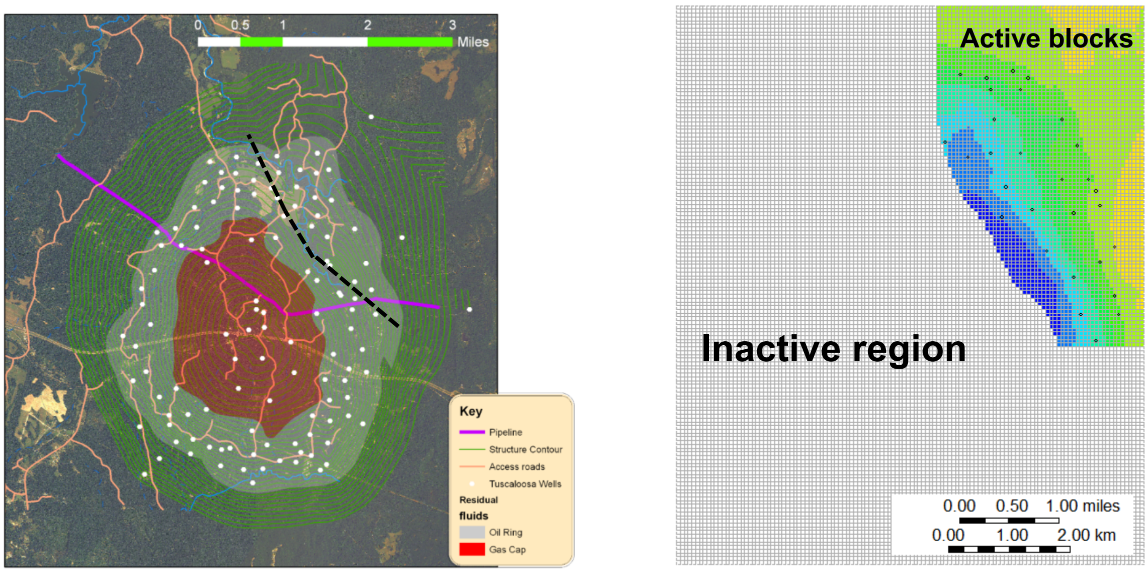

a) Cranfield site b) Simulation gridding

Figure 1-a) Structural contour map of Cranfield. The black dashed line represents the sealing fault that separates the northeastern section of the reservoir from the rest. b) Reservoir simulation model to simulate the CO_2 injection process. Simulation effort focuses on the northeastern side of the reservoir so the rest of model is inactivated to reduce the computational load. Color indicates depth, showing the structural trap formed against the fault.

Black oil models, although very efficient in less complicated cases, fail to address thermodynamics of CO_2/hydrocarbon interactions that are necessary to correctly simulate miscible processes at work at Cranfield. In this study, we employ the computer modeling group's (CMG) compositional simulator (GEM), an advanced general equation of state compositional simulator, designed for various complicated fluid flow problems including CO_2 miscible flood. The simulator was set up to model three fluid phases including water, oil, and gas.

The Peng Robinson equation of state (Peng and Robinson, 1976) is used in this study to model reservoir fluid properties. Our fluid model is composed of seven different components including CO_2. The thermodynamics model and component properties were tuned based on the fluid data published by Weaver and Anderson (1966). The data used for this purpose included bubble point pressure, solution gas-oil-ratio, formation volume factor, oil and gas viscosities. The CO_2/brine solubility in the current model is accounted for by using the Henry's constant. The experimental data from Duan and Sun (2003) are used to find the appropriate solubility parameters. Relative permeability curves are generated from the data published by Weaver and Anderson (1966). Keeping the residual values intact from the original relative permeability models, the relative permeability values at the endpoints were slightly modified to match the field production data. The slight modification of the relative permeability data (Figure 2) shows a agreement between the relative permeability set used in this study and the originally published data by Weaver and Anderson (1966).

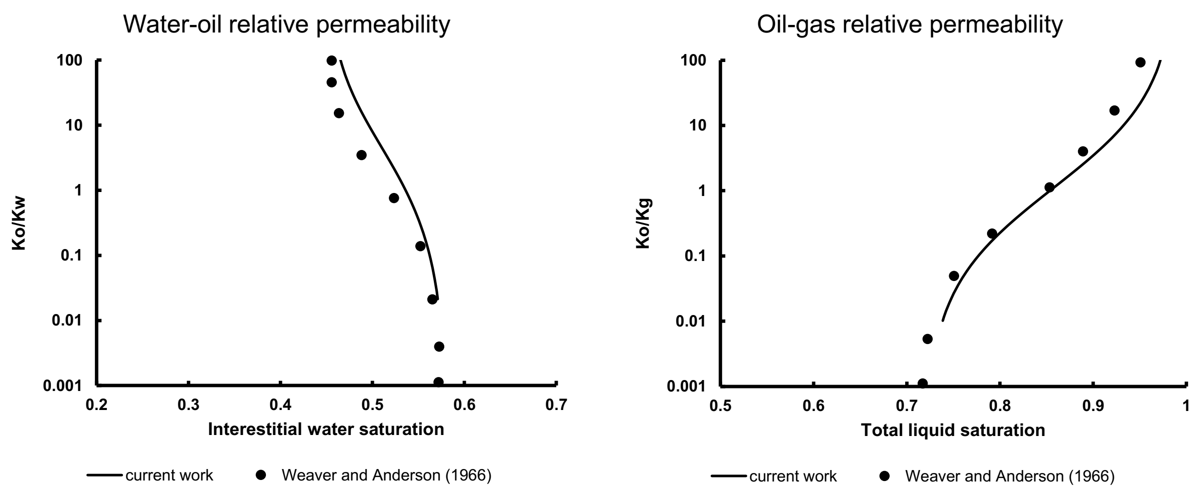

a) Water-oil relative permeability b) Oil-gas relative permeability

Figure 2-Relative permeability curves used in the current study are slightly modified from the original Weaver and Anderson (1966) values to match the oil, gas, and water production data during the CO_2 injection period. The new permeability sets are still in a good agreement with the original experiments.

The original permeability and porosity model is from Hosseini et al. (2013). They used a purely mechanistic approach to recognize eight different facies (flow zones) in the reservoir based upon combined permeability and porosity data sets. Each flow zone is given a porosity and permeability, which is constant for the entire zone. These flow zones are categorized under two main groups of low permeability (shale) and high permeability (sand) zones. High permeability channels in the lower Tuscaloosa Formation at Cranfield have been mapped and confirmed by various fluid-flow responses (Lu et al., 2013; Mukhopadhyay et al., 2015). However, the geometry of high permeability channels throughout the field presented by Hosseini et al. (2013) is based on probabilistic extrapolation of the available data. In this study, the permeability contrast between the sand and shale facies and the presence of high permeability flow paths was examined as a history matching parameter to fit the observed field data. Table 1 provides some of the more important reservoir properties used in this work.

Parameter	**Value**	**Parameter**	**Value**
Kh/Kv (permeability anisotropy)	0.05	Permeability range	0.016 – 4422 mD
Brine salinity	150,000 ppm	Porosity range	0.0002 – 0.45
Initial bubble point pressure	31.7 MPa	Irreducible water saturation	0.45
Original water oil contact depth	3064 m	Critical gas saturation	0.01
Original gas oil contact depth	3008 m	Aquifer model	Carter and Tracy (1960)

Table 1—Reservoir related parameters used in numerical modeling of Cranfield

2. History matching and reservoir performance

The first oil producing well from Cranfield was drilled in 1944. Since then, a productive area of about 7,750 acres was defined by 93 producing wells. The oil wells were drilled based on a 40-acres spacing while the spacing for the gas wells were 320 acres. The reservoir consists of an oil ring overlain by a large central gas cap (Weaver and Anderson, 1966). A cycling and condensate extraction plant was used to reinject the produced methane from Tuscaloosa and Paluxy reservoirs back into the gas cap. By 1951, the injected gas had broken through to many of the oil zone wells. The gas cycling continued until 1960 with dry gas sweeping the gas cap and the oil zone. Although the gas injection was intended to avoid, or slow down, the pressure depletion in the reservoir, reservoir pressure gradually fell below 27.6 MPa (4000 psi) causing water to encroach into the oil zone with increasing production. By the beginning of 1960, most of the wells had either a 100% water cut or a GOR greater than 100,000 scf/STB with an average field water cut equal to 88% and GOR equal to 85,000 scf/STB. The sale of gas cap methane and condensate started at that point. At the same time, water was produced in high volumes to prevent the aquifer from pushing the remaining oil into the gas cap. Gas injection stopped in 1964 when the project was near its economic limit. Production from the field was halted in 1966 and the reservoir was abandoned. Over the next several decades, a strong water drive restored pressure to near-initial levels.

Figure 3 shows the modeled oil and gas saturation in the abandoned reservoir after four decades of recovery, just before the initial seismic survey was conducted in 2007. According to the model, residual gas migrated toward the top of the structure and accumulated in a structural trap east of the sealing fault. The modeled residual oil saturations is as high as 0.35 is in the oil rim. As explained later, the presence of oil and gas with compressibilities larger than brine, can influence the sensitivity of seismic signals as CO_2 is injected. Therefore, it is important to quantify the amounts of residual oil and gas before conducting the seismic survey. No log or core-based measurements of hydrocarbon saturations from this pre-injection interval are available.

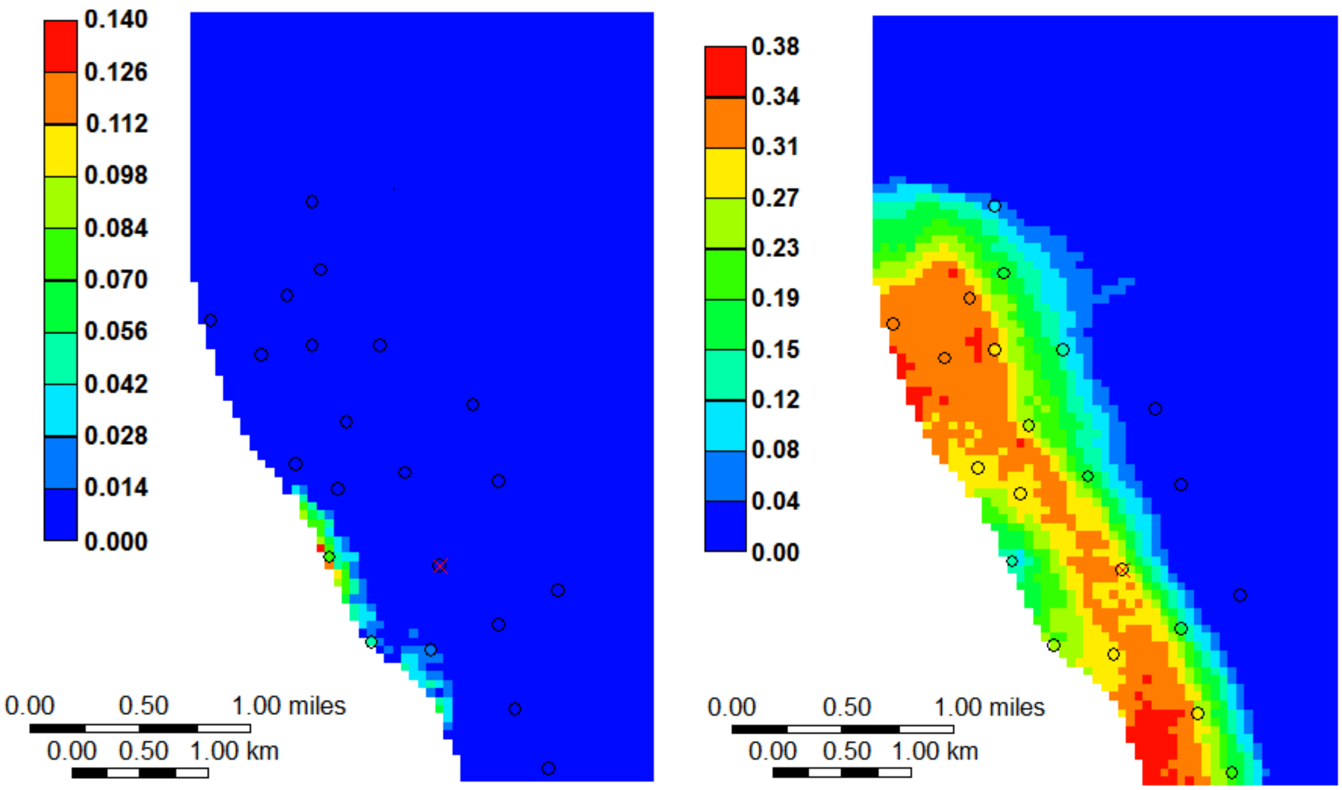

a) Gas saturation distribution at the time of baseline seismic survey.

b) Oil saturation distribution at the time of baseline seismic survey.

Figure 3- Modeled oil and gas saturation in the reservoir at the time of the first seismic survey in 2007.

In 2008, CO_2-based enhanced oil recovery (EOR) was initiated by Denbury Onshore, LLC to sweep the bypassed residual oil. Between 2008 and 2015, more than half of the oil ring (Figure 1a) was accessed using an irregular five-spot injection pattern with continuous CO_2 injection. Unlike many enhanced oil recovery efforts, there was no accompanying water injection at Cranfield. Initial patterns began in the northern part of the field and continued clockwise around the oil ring as the field was developed. CO_2 injection in the northeastern part of the reservoir commenced on July 2008 and continued until October 2012. Data gathered over 4 years of CO_2-EOR were used to calibrate the numerical model for a more reliable forecast of reservoir response. A total of 22 wells were considered for simulation of the northeast segment of the reservoir, 12 injection wells and 10 production wells. Injection wells were modeled based upon the injected CO_2 volumes available at each well location. To account for the amount of CO_2 entering the study area, a well located at the edges of the area of interest was modeled with half of the actual injection rate. The other half is assumed to enter that part of the reservoir that is not included in the model. Oil, water and gas productions rates were also available for all the producing wells during the simulation period. Monthly oil production rates were used as the operational constraint for the production wells. Cumulative production was calculated based on the fluid produced after July 2008. The history matching process in this section was based on observing/matching reservoir response by tuning the relative permeability data, adjusting the geological model to account for the high permeability zones, and altering the permeability contrast in high permeability channels in the reservoir. As discussed above, the presence of high permeability channels in the Tuscaloosa injection zone has been noted by other authors. Analyzing the breakthrough times (the time it takes for CO_2 to reach the production wells) confirms the presence of high permeability channels because CO_2 reaches some of the producing wells in a relatively short time after the start of injection, despite the spacing between the injection and production wells.

Figure 4 compares the cumulative oil, gas, and water production from the simulation and field data. The results show a reasonably good agreement between the field and simulation data, which accounts for the reliability of the numerical model to perform further analyses.

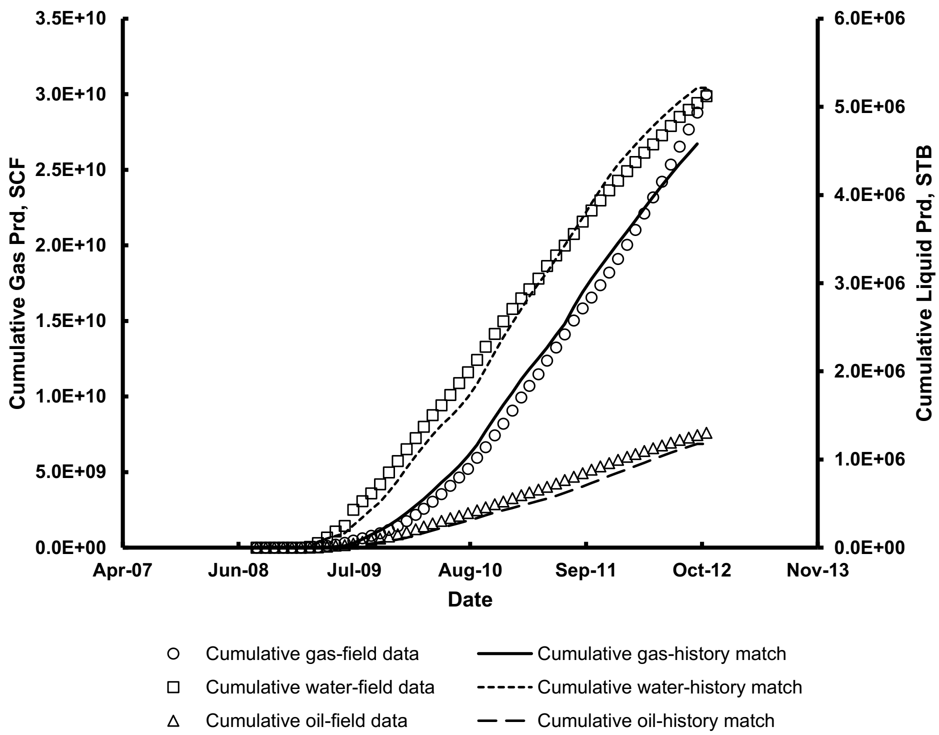

Figure 4-History matching results of 4 years' worth of production data shows an agreement between the field production data and simulation results.

As a way to verify the reliability of the simulation results, Figure 5 compares the CO_2 breakthrough times of the simulation with that of the field data. As we can see, the model is able to predict the CO_2 migration though the reservoir with an acceptable accuracy. This is significant because it implies that the modeled thickness and saturation between the wells are reasonable.

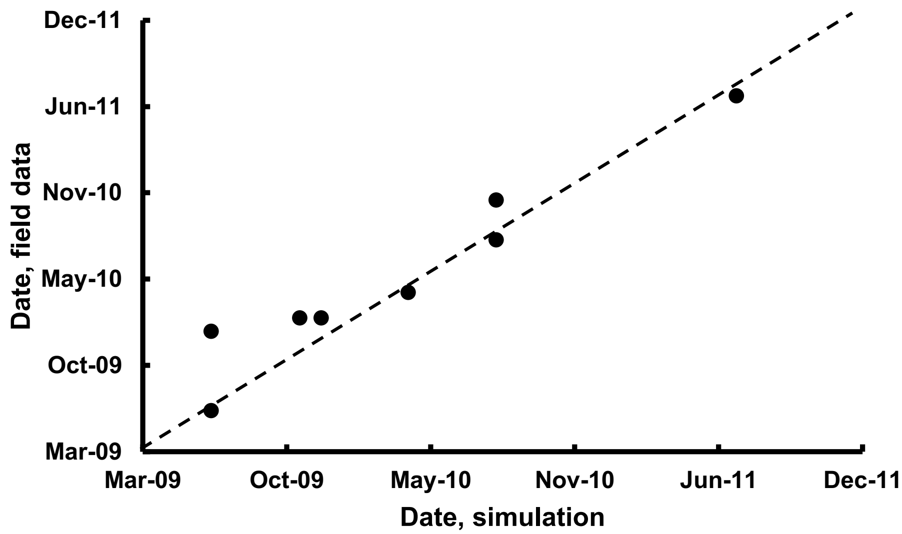

Figure 5-Breakthrough times for the producing wells show a good agreement between the simulation results and field data (x-axis shows the breakthrough times from simulation and y-axis shows that of real field data).

Next, we consider the CO_2 distribution after four years of CO_2 injection into the field. Figure 6 shows the average CO_2 saturation in the northeastern part of the reservoir at October 2012, the saturation of each plotted grid is averaged over the multiple vertical grids at that location. As is evident from the figure, carbon dioxide accumulates around the injection wells. CO_2 is also observed to migrate laterally and vertically below the former oil-water contact from the eastern and northern margins of the reservoir. New CO_2 injectors drilled near or below the oil water contact to assure that the base of the oil column was swept and to inject high volumes to support the SECARB project goals. High permeability in the lower Tuscaloosa channel facies also allowed migration below the oil-water contact as observed by (Lu et al., 2013). Looking at the average reservoir pressure from the simulation results ([Figure 7, Choi et al. (2011)), one notes that reservoir pressures rise as high as 37 MPa due to CO_2 injection. Such a high pressure in the reservoir can direct CO_2 into the lower pressure edges of the reservoir where the aquifer pressure is around 32 MPa, resulting in CO_2 migration off the structure.

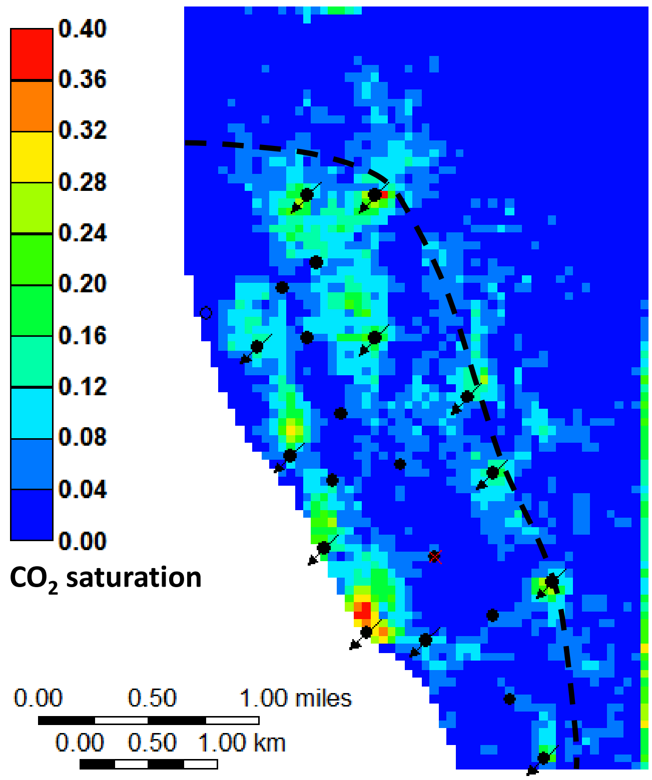

Figure 6-Modeled CO_2 saturation distribution map at October 2012 shows CO_2 accumulated around the injection wells (black dots with arrows). CO_2 saturations of each grid cell is averaged over the local thickness of the zone. Water-oil contact illustrated by dash line.

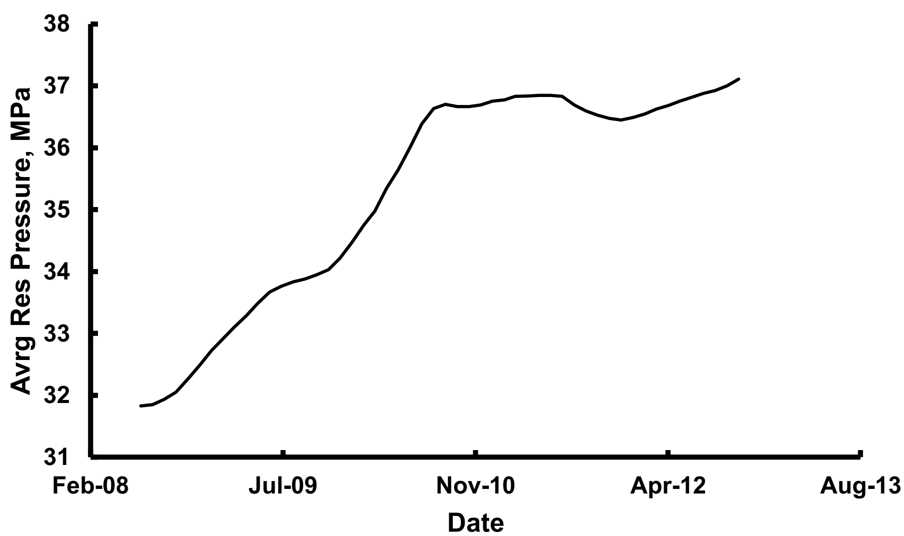

[Figure 7-Reservoir pressure increases after CO_2 injection commences at 2008, providing a driving force to move CO_2 below the original oil-water contact.

2. Seismic data interpretations

The changes in fluid saturations due to the injection and production operations at the Cranfield site lead to seismic velocity variations within the reservoir. Such changes can induce temporal differences in the amplitude of reflections from the top of the reservoir and within the reservoir itself. In addition, the velocity changes may induce time shifts in reflections within and below the reservoir. Such time shifts will lead to apparent amplitude changes as one set of reflections is offset in time from the other. In an effort to image seismic velocity variations associated with the injection of more than 2 million tons of CO_2, two seismic surveys were collected, the base survey in 2007 before the start of injection and a follow-up survey in 2010. The two surveys were processed by the commercial contractor Geotrace following identical workflows. The changes in the seismic response between the two surveys have been analyzed previously by Zhang et al. (2013, 2012), Ditkof (2013), and Carter (2014). The pattern of amplitude changes is complicated and there is an imperfect correlation between areas where CO_2 was injected and locations of seismic amplitude changes. This shows a limitation in using the 4-D seismic to assess the distribution of CO_2 as well as using it to validate the fluid flow model.

Because the seismic amplitude response depends upon both the changes in the reflection coefficients and velocity-induced time-shifts of the peaks and troughs of the seismic traces, it may not have a simple relationship to velocity changes in the reservoir. As an alternative, we use the simpler method of interpreting the time shifts in the seismic traces. Ignoring any stress and strain changes in the reservoir amplitude changes should be directly related to velocity changes. To this end, we examined the time shifts between traces of the two seismic cubes produced by Geotrace. This approach is somewhat similar to the work of Ditkof (2013) but the implementation is significantly different. In particular, Ditkof (2013) used two large time windows from 0.35 to 1.80 s above the reservoir and 2.50 to 3.20 s below the reservoir. The lower time window is substantially below the reservoir and is likely to be influenced by a number of factors related to the seismic processing. Any time shift due to velocity changes in the reservoir should begin just below the reservoir and extend to a large distance below it. In an effort to isolate the time shift due to velocity changes within the reservoir, we line up traces using a time window of 0.20 s, extending upward from the top of the reservoir (Figure 8). The segments of the two traces are aligned by cross-correlating them to produce a cross-spectrum (Figure 9). To obtain sub-sample precision we fit a quadratic polynomial function to the five points surrounding the peak of the cross-spectrum. Such local approximations are often used in determining minima and maxima, as quadratics are the lowest degree polynomials that can represent a single extremum. A linear form cannot represent a peak or a trough and a higher-order polynomial would introduce additional extrema. The time delay associated with the peak of the quadratic is used as the time shift. Once the traces are aligned in the window above the reservoir, the shift is applied to the segments of the traces in the window below the reservoir. Then, the relative shift is computed for these corrected traces using the cross-spectrum and the quadratic fitting technique.

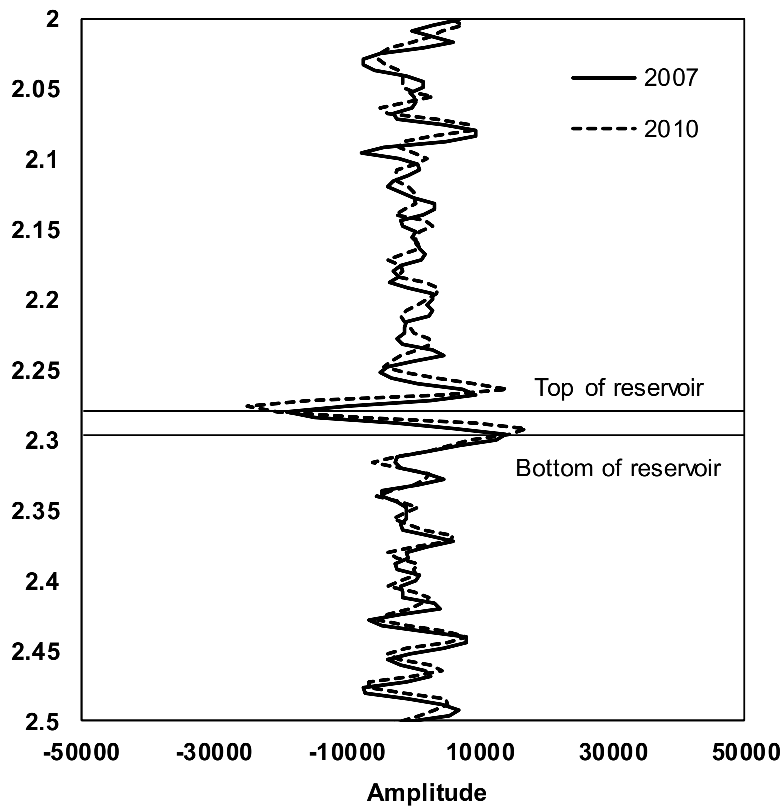

Figure 8- Two traces from the baseline (2007) and follow-up (2010) seismic surveys. The top and bottom of the reservoir are indicated by the horizontal lines.

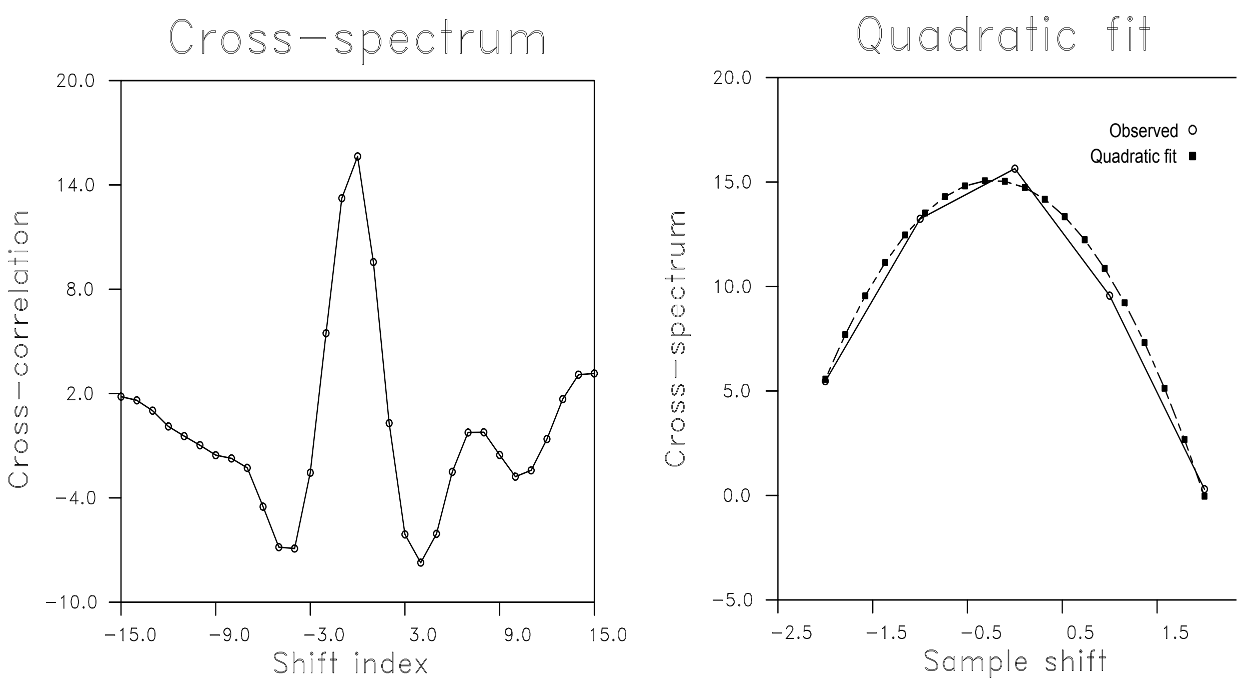

(a) (b)

Figure 9-a) Cross-spectrum of the segment of the two traces for the window above the reservoir. The magnitude of the cross-correlation is plotted as a function of the shift. b) Quadratic fit (filled squares) to the five points surrounding the peak.

The approach was applied to every location for which there were traces for both the 2007 and 2010 surveys. Figure 10a shows the time shifts for the northeastern side of the reservoir. The regions with greater time shifts indicate areas where there has been larger changes in acoustic properties, primarily because CO_2 has replaced the reservoir fluid (either oil or brine). On the right side of Figure 10b we show the simulated CO_2 saturation at the time of the second seismic shoot (2010). The black circles in Figure 10b provide the locations of injection wells. Larger radii indicate more CO_2 injection. Field development and CO_2 injection commenced from the northern part of the study area, so more CO_2 has accumulated in those regions (larger circles). Comparing the history-matched simulation results with that of the seismic interpretations, one can claim that the seismic data provides a reasonable estimate of the CO_2 plume and its areal extent. In fact, the agreement suggests that time-lapse seismic surveys may be used to monitor subsurface CO_2 injection, provided that the actual physical characteristics of the site does not limit the applicability of seismic methods, and data acquisition and interpretation methods are optimized with respect to the problem specifications.

The time-lapse seismic map (Figure 10a) shows larger increases in time shifts in regions where higher amounts of CO_2 have been injected (Region A in the map). In fact, the greater the volume on injected CO_2 injection, the more pronounced the variation of the acoustic properties should be. According to Figure 10b, the amount of CO_2 injected in this region is less than the average amount in Region A. Hence, fluid properties in this region do not change as much as in Region A, resulting in a lighter alteration in acoustic properties in this region. As a result, although the time-lapse maps show a slight alteration of the acoustic properties in this particular region, the variations are not as intensified as Region A. It is important to add that there have been different interpretations of the same seismic data from Cranfield (Alfi and Hosseini, 2016). The main difference between the current interpretation and the ones done by other authors is that the previous interpretations appear to underestimate the changes in the region around the sealing fault (Region B). In other words, although the volume of injected CO_2 in Region B is less than the volume injected into Region A, the current seismic interpretations reveal a detectable change in seismic responses from Region B. It worth to mention that the previous efforts failed to identify any significant changes occurring in Region B. The next section discusses some of the possible reasons for a weak signal in the structural trap east of the fault (Region B).

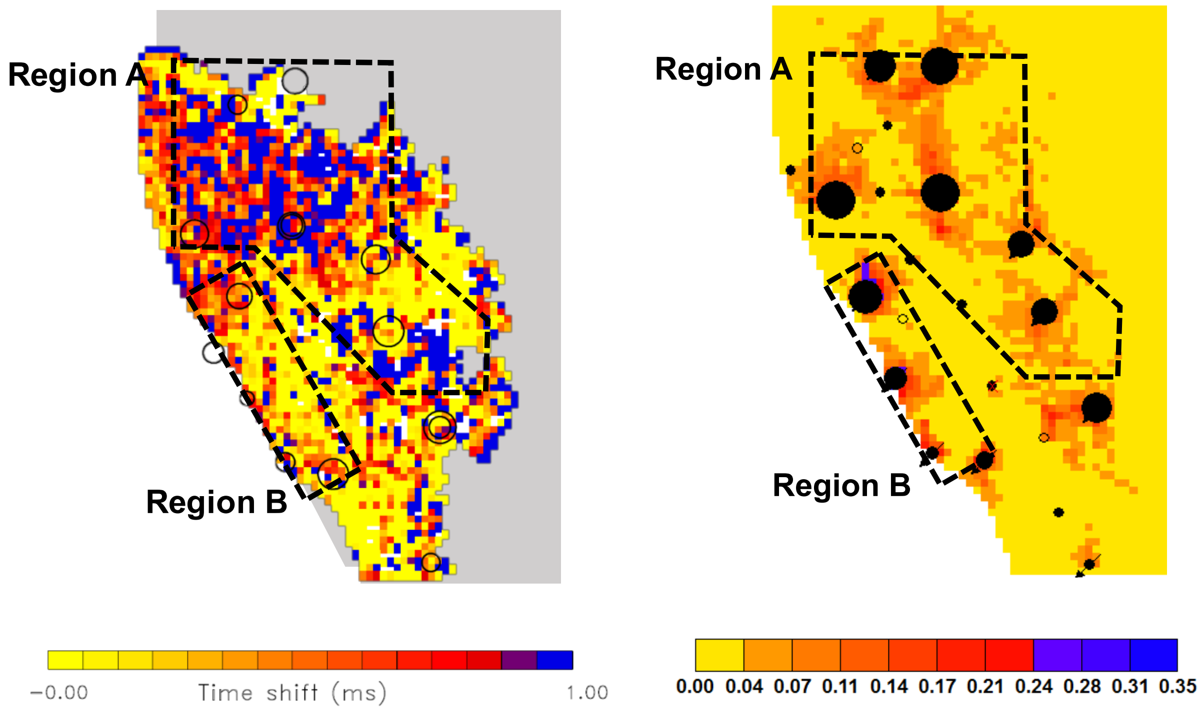

a) Time shift map after CO_2 injection (seismic data)

b) Modeled average CO_2 saturation map (simulation) over local thickness.

Figure 10-Seismic time shifts compared to the simulated CO_2 saturation distribution (both maps show the study area on September 2010). Time shifts are more pronounced in regions with a higher CO_2 saturation. The simulated saturations are averaged over the local thickness of the reservoir. The circles show the location of wells where the larger circles indicate higher amount of injected CO_2.

3. The curious case of Cranfield

In this section, we provide a heuristic discussion of the Cranfield case, beyond the simple observation that areas with higher volumes of injected CO_2 should be detected in the seismic surveys. A Weaker seismic time-lapse signal in Region B is not only attributed to less total injected CO_2 in that region, but also to the actual physics of the problem. Factors that we consider here include zone thickness and pre-injection fluid composition. In cases where the injection zone is thin, lower resolution seismic surveys may not be able to detect the changes properly and any possible signal change will be diluted by intact overlying/underlying layers with no injected CO_2. In other words, a signal from the thin CO_2 invaded zone will be mixed with the weaker response of the nearby layers and the composite signal does not represent the actual change in elastic properties of the porous media induced by CO_2 injection. For the case of Cranfield, the thickness of the CO_2 plume is somewhat uncertain because of non –ideal sweep efficiency at this early stage of injection in the heterogeneous reservoir. However, the operator placed several injection wells within the structural trap produced by the sealing fault, in expectation of a thick oil column target below a small gas cap (Figure 3). Figure 11 shows the productive thickness of the oil zone in Basal Tuscaloosa Sand, Cranfield unit. As we can see, the reservoir thickness in Region B, where seismic signals were relatively weaker is comparable to that of the rest of the oil zone.

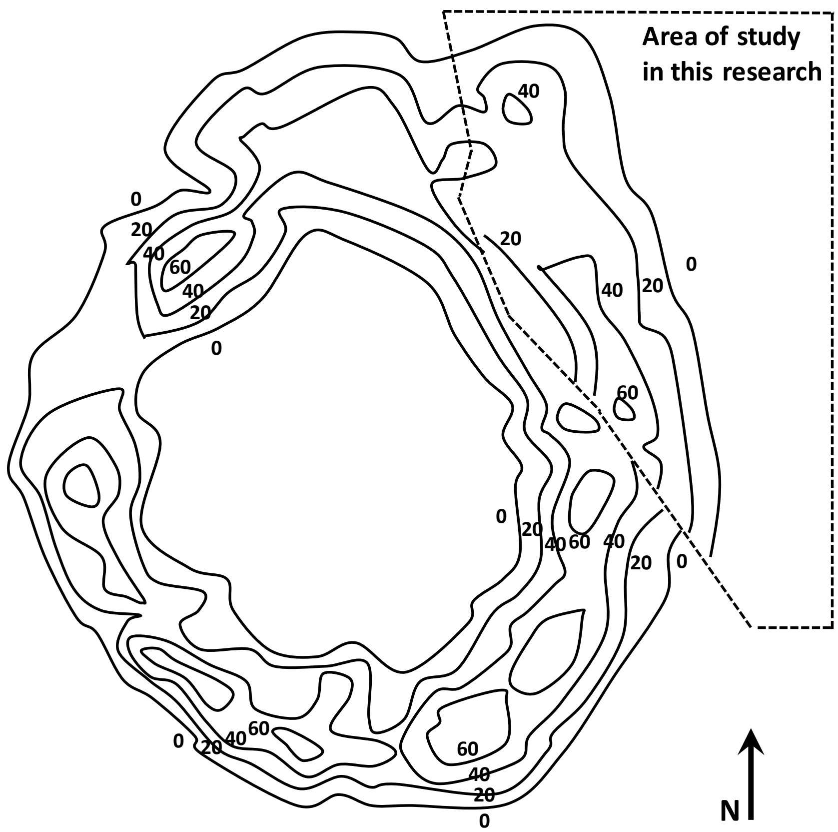

Figure 11-The productive zone thickness map of the study area (denoted by dashed polygon) shows the pay zone in the area of interest, located close to the sealing fault, which has a relatively high thickness compared to the other regions of the oil zone (contour map regenerated after Weaver and Anderson (1966)).

Seismic signals may also be influenced by the presence of gas, specifically methane, in the formation. It is informative to consider the gas saturation distribution prior to the first seismic survey at 2007 (Figure 3a). Given the prior production history, the most effective way to evaluate this is through a compositional reservoir simulation. According to the map of modeled gas saturations, the gas that has evolved in the reservoir during the primary production period (1944-1964) will move up-dip towards the center of the reservoir and will accumulate near the trap to the east of the sealing fault. The presence of even small gas concentrations during the first seismic survey can cause masking effects in which the alteration in acoustic properties of the reservoir are not large enough to be detectable during the repeat seismic survey, particularly for a case with a relatively high noise ratio.

To understand the reasoning behind such behavior, we turn to rock physics modeling and fluid substitution theory (Mavko et al. 2009). Fluid substitution uses seismic velocities in rocks saturated with one fluid to predict cases where the rock is saturated with a second fluid (here CO_2), or equivalently predicting saturated rock acoustic velocities from that of dry rocks. Fluid substitution provides the interpreter with a tool for modeling and quantifying the different fluid replacement scenarios, which might give rise to the observed amplitude and travel time variation in the time-lapse responses. The most commonly used approach for fluid substitution calculations is the low-frequency approach known as Gassmann's fluid substitution (Gassmann 1951). To model the changes from substituting one fluid with another we should first remove the effects of the initial fluid and replace it with the new fluid. Gassmann's primary equation correlates the saturated bulk modulus of the rock to its porosity and the bulk moduli of the porous rock frame, mineral matrix, and the pore filling fluids (Smith et al., 2003):

$$K_{\mathrm{sat}} = K^* + \frac{\left(1 - \frac{K^*}{K_0}\right)^2}{\frac{\phi}{K_{\mathrm{fl}}} + \frac{1-\phi}{K_0} - \frac{K^*}{K_0^2}} \qquad (1)$$

where K_{sat} represents the bulk modulus of the porous media saturated with the fluid of interest, K^* is the bulk modulus of the porous rock frame (with no fluid inside the pores), K_0 is the bulk modulus of the mineral matrix (depends on the minerology of the rock components), K_{fl} is the pore-filling fluid's bulk modulus, and ϕ is porosity. In this formula, the value of K^* does not depend on the fluid properties. To use this equation, the rock is drained of the initial fluid to determine the bulk and shear moduli of the porous frame (K^*). The porous frame properties are then used to calculate the new effective bulk modulus of the media saturated with the new fluid (K_{sat}). Gassmann equation assumes a connected pore space with equilibrated pressure along the pore network.

When the fluid saturation in a porous media varies, for example as CO_2 replaces oil or water in the reservoir, the fluids can distribute within the formation in various configurations and this can lead to different bulk moduli (K_{sat}) for the fluids. For example, in the case of a uniform or homogeneous distribution of fluids, the new value of K_{fl} is computed using the Reuss average (Smith et al., 2003):

$$K_{\text{fl}} = \left[\sum \frac{S_i}{K_i} \right]^{-1} \quad (2)$$

where S_i represents the saturation of each individual fluid while K_i is the bulk modulus of that fluid phase. Eq. 2 is the effective modulus for a stack of layers perpendicular to the direction of propagation of the seismic wave. The Reuss average is also a lower bound on the effective fluid bulk moduli because the weakest layer determines the modulus. Note that the assumption of a homogeneous fluid distribution or of fluids arranged in layers perpendicular to the direction of propagation is not always a good approximation. While we cannot consider all of the possible fluid arrangements, we can consider the other extreme distribution that gives an upper bound on the effective fluid bulk modulus. This modulus, known as the Voigt bound, is given by

$$K_{\text{fl}} = \sum S_i K_i \quad (3)$$

and corresponds to the case in which the fluid is arranged in layers oriented parallel to the direction of propagation (Mavko et al., 2009). In that case the strongest layers determine the effective modulus. Given that one typically does not know the distribution of fluid in a heterogeneous reservoir with an extensive history of production and injection, we cannot be certain about the averaging that we should use. However, in making estimates of seismic velocity changes due to fluid saturation one could compare both the Reuss and Voigt approaches in order to gauge the possible variation. The Hill estimate, which is simply the average of the Reuss and Voight bounds, represents a reasonable approximation to the fluid bulk modulus in the face of uncertainty regarding the nature of the saturation distribution within a given reservoir (Mavko et al. 2009).

Changing K_{fl} would ultimately affect the bulk modulus of the saturated porous media (K_{sat}). When K_{sat} changes, the seismic velocities in the reservoir would change and such changes can be detected in the time-lapse surveys and are interpreted as variation in fluid content of the reservoir. Eq. 4 shows how p-wave velocities are related to the saturated bulk modules of the porous media:

$$V_{\mathrm{p}} = \sqrt{\frac{K_{sat} + \frac{4}{3}G}{\rho_B}} \tag{4}$$

In this equation, V_{p} is the p-wave velocity of the saturated media, G is the shear modulus of the saturated media and ρ_{B} is the bulk density (fluid and rock). Note that the shear modulus (G) does not depend on the fluid content and will not vary with reservoir fluid alteration. Gassmann's fluid substitution will affect the value of V_{p} by changing K_{sat} and ρ_{B}. In Figure 12 we plot the seismic velocity variations corresponding to Reuss and Voigt approaches to averaging the fluid moduli. In addition, we also plot the Hill estimate, which is just the arithmetic average of the two bounds.

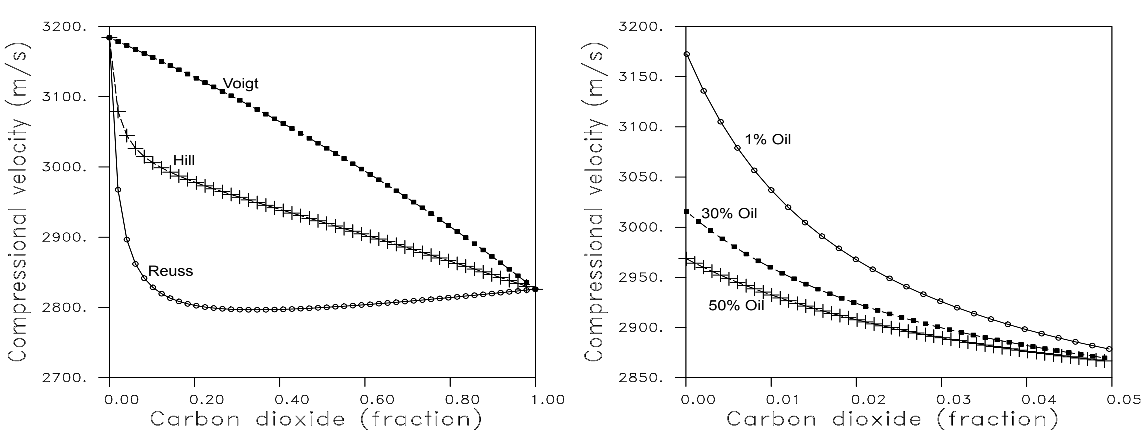

(a) (b)

Figure 12-a) Voigt, Reuss, and Hill based estimates of compressional velocity changes in a porous layer saturated with varying fractions of carbon dioxide and water. b) Effect of varying

oil saturation as a third contribution to the fluid mixture for the Reuss average. The horizontal scale indicates the fraction of carbon dioxide trading off with water content.

To understand the importance of the presence of residual gas and its effect on seismic velocity, and to mimic the situation at Cranfield, consider a simple model in which the reservoir has a porosity of 0.24 with the mineral frame primarily composed of quartz. Ditkof (2013) reported an average P- and S-wave velocities of 3328 and 2096 m/s for a 100% brine saturated rock in this deposition environment (S- and P-velocities are used to calculate the bulk modulus of the porous rock frame, K^*). According to Mavko et al. (2009), quartz has a bulk modulus of 36 GPa and density of 2.65 g/cc. Now, consider a case in which the reservoir is initially saturated with 40% water and 60% oil and CO_2 is injected into the reservoir to replace oil. **Error! Reference source not found.** uses the Gassmann formula and Reuss average to calculate the p-wave velocities for different injected CO_2 saturations. According to the graph, 30% increase in CO_2 saturation (from 0 to 30) will cause P-velocity to decrease from 3170 to 3010 m/s, which is 160 m/s reduction in the V_p. Now consider a case in which the reservoir is originally saturated with 40% water, 50% oil, and 10% residual gas. To make the case easier to understand and to be able to still use **Error! Reference source not found.**, we will assume the residual gas in the reservoir (usually methane or low-end light hydrocarbons) have properties comparable to that of CO_2 so we can still use the P-wave velocities in **Error! Reference source not found.**. For this case, the initial P-wave velocity (before any CO_2 is injected) should be read at the gas saturations of 10%, due to the presence of residual gas. According to the graph, the initial V_p is around 3040 m/s. Now assume we inject CO_2 in the reservoir and add 30% to the gas saturation in the reservoir. The repeat seismic survey in the area of the CO_2 injection will read a P-wave velocity of 3005 m/s (at CO_2 saturation of 40%). This means, 30% increase in CO_2 saturation will decrease the P-wave velocity by only 35 m/s. When we compare this value to the original reduction of 135 m/s for cases with no residual gas in the reservoir, one can conclude that the variation in elastic properties can be masked when residual gas is present in the reservoir. This is important because seismic surveys always contain random and signal-generated noise. If the level of expected changes in seismic responses is comparable to the noise level, such changes could be completely obscured. A similar masking effect is reported by Urosevic et al. (2011) when injecting CO_2 into a depleted gas reservoir in the

Otway Basin, Australia. Their results showed that presence of residual gas impacts changes in elasticity of the reservoir rock after CO_2 injection in which even carefully implemented time lapse seismic methodologies are not capable of capturing the changes.

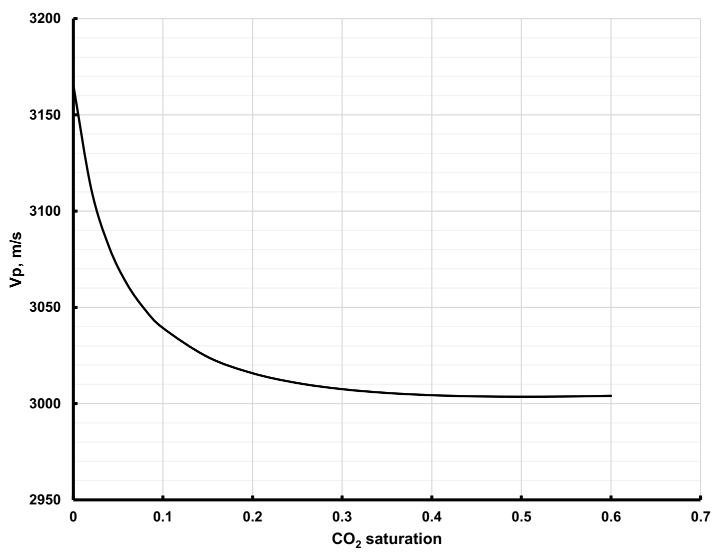

Figure 13-P-wave velocity in the saturated media decreases as CO_2 (fluid with a lower bulk modules) saturation increases. Seismic wave velocity decline is steeper for lower saturations and slows down as CO_2 saturation increases, according to the Gassmann formulation.

Pressure changes in the reservoir, due to injection and production can also lead to changes in seismic velocity. This may be due to changes in the bulk moduli of the rock matrix induced by variations in effective pressure, or by changes in the nature of the fluid. For example, if the fluid pressure is lowered below the bubble pressure gas may ex-solve from the solution. Recently, the velocity-stress sensitivity at Cranfield has been characterized using crosswell seismic data (Marchesini et al. 2017). This continuous active-source monitoring experiment during fluid withdrawal indicated that the fractional change in seismic velocity for a given change in fluid pressure is given by

$$\frac{\frac{dV}{V}}{dP} = \frac{\frac{dt}{T}}{dP} = 1.09 \times 10^{-3}/MPa$$

In order to calculate the influence of pressure changes on the seismic travel time and velocity changes we considered the pressure variations calculated by the numerical reservoir simulation. The estimated pressure changes between the two seismic surveys in 2007 and 2010 are shown in Figure 14.

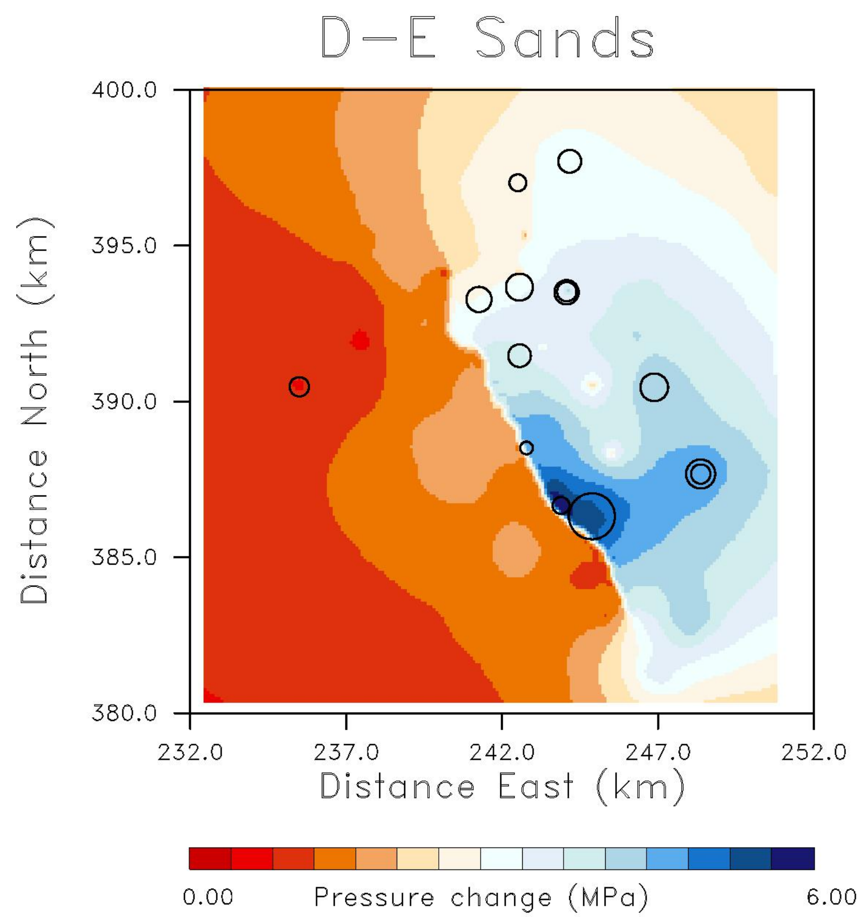

Figure 14. Pressure changes between the seismic surveys in 2007 and 2010, calculated using the compositional reservoir simulation.

Given the pressure changes within the reservoir, we estimate that the change in two-way travel time through the reservoir will be less than 0.1 ms and that the change in velocity will be less than 1%. As is evident in Figure 14, this change will be largest in an area adjacent to the bounding fault and much less outside of this region. Furthermore, it has been hypothesized that the change is due to gas coming out of solution due to the pressure decrease during the pumping test. Thus, given that the pressure increases within the reservoir during the injection of carbon dioxide, the seismic changes due to such pressure variations might be much smaller. Given that the time shifts estimated from the time-lapse data are of the order of 1 ms, the pressure changes are not thought to significantly impact our results.

4. Comparison of different seismic interpretations from Cranfield

In this section, we compare the results of three different interpretations from the same seismic data acquired from Cranfield (Figure). This comparison helps us to understand how the actual physics of the problem can influence our interpretation of the same seismic data. In Figure a, five injection wells are marked with letters A to E. The color map shows average CO_2 saturation at the time of the second seismic survey (2010) and the size of the black circles show the relative amount of CO_2 injected into the ground. In Figure 15, the letters are selected in a way that they are geographically consistent in all four graphs. If the seismic interpretation works as predicted, time-lapse seismic signals should show a more pronounced change in those injection locations. Figure b represents the seismic interpretations from the current work. Figure c shows the amplitude change map by flattening the reservoir to 2300 ms to characterize a 4D response (Ditkof et al., 2011; Ditkof, 2013). A relatively high amount of noise was reported in the seismic data, which can influence the repeatability of analysis according to the authors. Carter (2014) used the 3D seismic data along with well logs to probabilistically invert the CO_2 saturation and porosity distribution in Cranfield (Figure d). The well logs were used to calibrate the rock-physics model, which later was used to statistically derive the porosity distribution. A high resolution basis pursuit inversion was then used to invert seismic data for P-impedance and obtain the CO_2 saturation distribution (Carter, 2014).

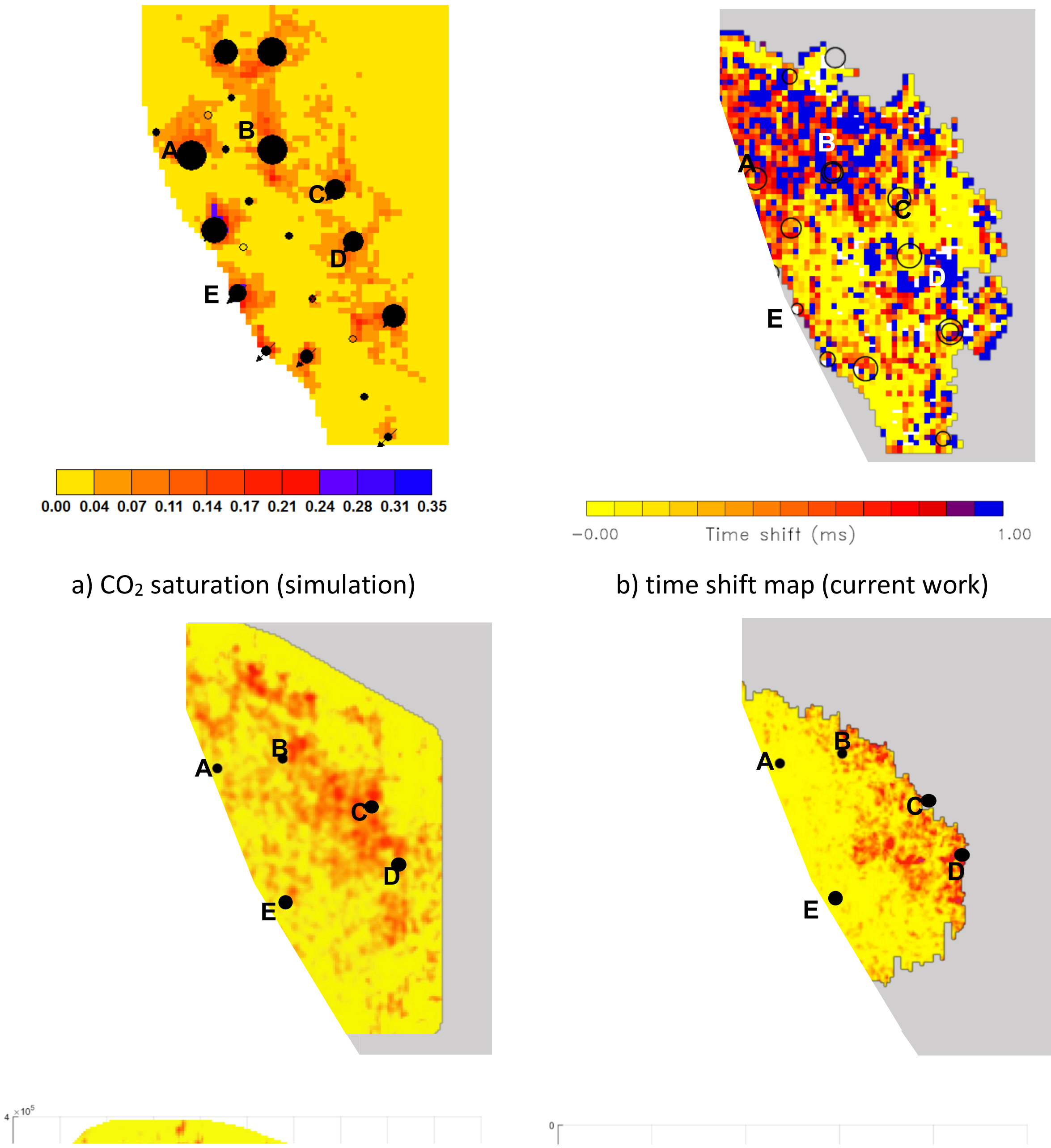

a) CO_2 saturation (simulation)

b) time shift map (current work)

c) amplitude change map (Ditkof et al., 2011)

d) CO_2 saturation from seismic (Carter, 2014)

Figure 15- Comparison of Cranfield seismic interpretations from three different studies with the actual field injection data and reservoir simulation results.

Let us consider point A where field data and simulation results show a considerable amount of injected CO_2 with high CO_2 saturations around an injection well. The new seismic evaluation from this paper (Figure b) shows a noticeable change in the time shift around point A, while the interpretations by Ditkof et al. (2011) (Figure c) and Carter (2014) (Figure d) do not. This represents an example of an improvement in seismic interpretation that results in an improved match with the fluid flow model. CO_2 injection in points B and D is captured in all three seismic interpretations. These matches increase confidence in the correctness of the fluid flow model and the seismic interpretation. Both Ditkof et al. (2011) and Carter (2014) report no alteration in elastic properties of the media. We believe that correlates to the specific physics of the current problem, in which presence of residual gas migrated to the top of a structural trap adjacent to the sealing fault, which can mask the seismic signals in that area. However, some smaller scale mismatches remain; for example at point D, we can see a mismatch between the new seismic interpretation and the fluid flow model. The reservoir is highly heterogeneous and it is not possible to characterize it on a small enough scale to adequately capture this variability. The history matching of production data can capture the larger-scale variations in reservoir properties but will likely miss variability that is important for the detailed changes in seismic properties. In addition to the variability in static flow properties, there are variations in fluid saturations due to past production and injection. This will lead to spatial variations in the distribution of methane, water, and oil within the reservoir, variations in the thickness and geometry of the zone saturated by CO2, in addition to variations in both mechanical and flow properties. Therefore, we might only expect to obtain large-scale agreement between reservoir simulation predictions and observations of seismic time-lapse changes.

5. Forward model

In an effort to capture some of the large-scale variability that is possible in the seismic time-shifts, we used the simulation estimates of total saturation methane, water, oil, and carbon dioxide in 2007 and 2010 and Gassmann's approach to estimate seismic velocity changes within the reservoir. A background velocity model was constructed from three well logs that contained compressional velocity sonic logs to construct an average model. The velocity changes were superimposed on this background model for each location within the seismic velocity cube to construct a series of one-dimensional vertical profiles. Each linear profile was subject to a variable scale change in order to match the location and thickness of the reservoir boundaries. An approximate reflection response for a vertically propagating wave impinging on a stack of elastic layers was computed using the method of Kennett (Kennett, 1983, 1974). We considered the three methods discussed above for averaging the saturations and fluid bulk moduli in order to compute the effective fluid bulk modulus, namely the Reuss, Voigt, and Hill averaging techniques. The resulting time shifts computed from the synthetic seismograms are shown in Figure . It was found that the most significant effects were due to the locations of interaction of injected CO_2 with the oil-water contact at the edge of the field. Large changes were found in two main areas: where CO_2 replaced brine in the water leg and in the area of high CO_2 accumulation in the structural trap at the sealing fault. The relative size of the time shifts varies, depending on the technique used to average the fluid moduli (Figure). For the Reuss model the largest changes are in the water leg to the northeast. For the Voigt approach the most significant changes are near the bounding fault. If the Hill method is used then the two major anomalies, near the bounding fault and in the surrounding aquifer, are roughly equal in magnitude. Note that the Voigt model leads to time shifts that are about an order of magnitude lower than the observed values. As mentioned earlier, the Reuss model would appear to be more compatible with property distributions that are largely horizontal or sub-horizontal.

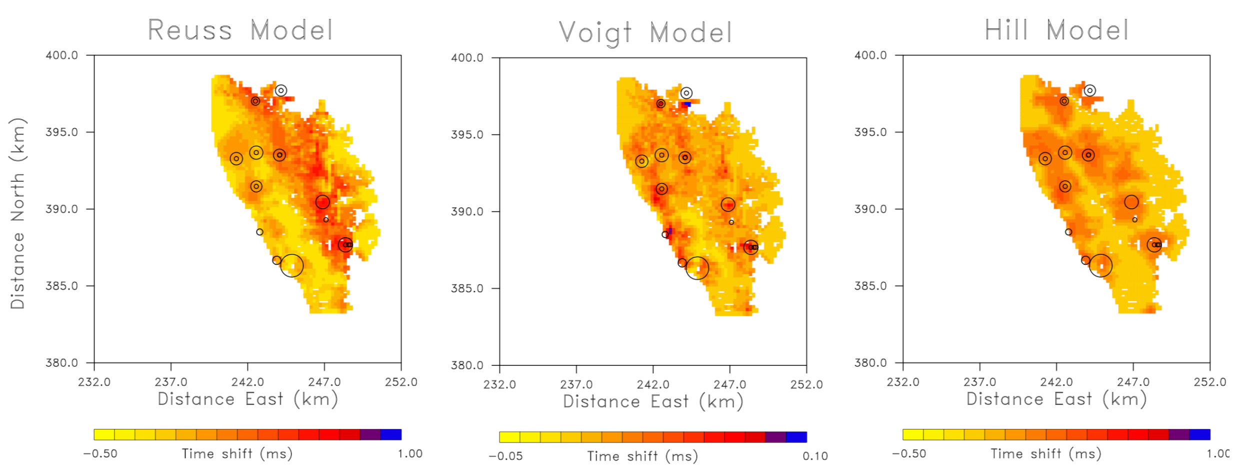

(a) (b) (c)

Figure 16-Time shifts calculated using the reservoir simulations and computed changes in methane, oil, water and carbon dioxide saturations. Three different methods, the Reuss bound (a), the Voigt bound (b), and the Hill average of the two (c), were used to compute the effective fluid bulk modulus at each location in the reservoir. Please note that time shift color scale is variable in different plots.

In general, the calculated time shifts (Figure) are in qualitative agreement with the observed values (Figure 10 and Figure) with large changes in the water leg of the reservoir and smaller but observable changes in the trap near the bounding fault. The detailed distribution of the anomalies will depend upon smaller scale variations in reservoir properties and will be influenced by heterogeneous static properties as well as variations in background fluid saturations due to earlier production and injection. It may be possible to use the good quality seismic data to infer these properties but that would be difficult with just a single pair of low resolution seismic surveys. In absence of economic limitations, a more robust approach would be to use a number of seismic surveys to image the propagation of the changes and to infer the onset of changes in the seismic properties due to the propagation of the carbon dioxide. Such onset times are more sensitive to flow properties and less sensitive to the rock physics models that govern the mapping from saturations to seismic moduli (Vasco et al., 2015, 2014). Multiple surveys were used at the Sleipner site (Arts et al., 2004) and they clearly documented the movement of the carbon dioxide in three dimensions.

Conclusions

In this paper, we compared the results of reservoir simulation and seismic interpretation to consider a strategy for determining CO_2 movement during EOR operations. A compositional simulation approach is employed to address thermodynamics of CO_2/hydrocarbon interactions and reliably model the miscibility phenomenon. Of a specific interest is gas exsolution/dissolution, which essentially leads to accurate modeling of gas appearance in the reservoir. The numerical model is history-matched using the available field production data. Seismic interpretations show large changes in the water leg of the reservoir and smaller but observable changes bordering the structural trap against the bounding fault. We obtain large-scale agreement between reservoir simulation predictions and observations of seismic time-lapse changes. In addition to the variability in static flow properties, there are variations in fluid saturations due to past production and injection. This will lead to spatial variations in the distribution of methane, water, and oil within the reservoir, in addition to variations in both mechanical and flow properties. For the specific case of Cranfield, one can conclude that the variation in elastic properties (before and after CO_2 injection) can be masked when residual gas is present in the reservoir. This is important because seismic surveys often come with uncertainty and noise and if the level of expected changes in seismic responses is comparable to the noise ratios, such changes could be completely ignored or misunderstood.

Acknowledgments

The authors thank Computer Modeling Group for providing the academic license for CMG-GEM. Publication authorized by the Director of the Bureau of Economic Geology, the University of Texas at Austin. Research funded in part through National Energy Technology Laboratory DOE award number: DE-FC26-05NT42590 to the Southeast Regional Carbon Sequestration Partnership, managed by Southern States Energy Board. D. W. Vasco would like to acknowledge the support of the U. S. Department of Energy under contract number DE-AC02-05CH1123.

References

Alfi, M., Hosseini, S.A., 2016. Integration of reservoir simulation, history matching, and 4D seismic for CO2-EOR and storage at Cranfield, Mississippi, USA. Fuel 175, 116–128. https://doi.org/10.1016/j.fuel.2016.02.032

Alfi, M., Hosseini, S.A., Alfi, M., Shakiba, M., 2015. Effectiveness of 4D Seismic Data to Monitor CO2 Plume in Cranfield CO2-EOR Project, in: Carbon Management Technology Conference. Carbon Management Technology Conference. https://doi.org/10.7122/439559-MS

Arts, R., Eiken, O., Chadwick, A., Zweigel, P., van der Meer, L., Zinszner, B., 2004. Monitoring of CO2 injected at Sleipner using time-lapse seismic data. Energy 29, 1383–1392. https://doi.org/10.1016/j.energy.2004.03.072

Carter, R.D., Tracy, G.W., 1960. An Improved Method for Calculating Water Influx.

Carter, R.W., 2014. Fluid Characterization at the Cranfield CO_2 Injection Site : Quantitative Seismic Interpretation from Rock-Physics Modeling and Seismic Inversion.

Choi, J.-W., Nicot, J.-P., Meckel, T.A., Hovorka, S.D., 2011. Numerical modeling of CO2 injection into a typical US Gulf Coast anticline structure. Energy Procedia 4, 3486–3493. https://doi.org/10.1016/j.egypro.2011.02.275

Davis, T.L., Terrell, M.J., Benson, R.D., Cardona, R., Kendall, R.R., Winarsky, R., 2003. Multicomponent seismic characterization and monitoring of the CO2 flood at Weyburn Field, Saskatchewan. Lead. Edge 22, 696–697. https://doi.org/10.1190/1.1599699

Ditkof, J., Meckel, T.A., Zeng, H., Hovorka, S.D., 2011. Time lapse seismic response (4D) related to industrial-scale CO2 injection at an EOR and CCS site, Cranfield, MS. Am. Geophys. Union, Fall Meet. 2011, Abstr. #GC51B-0976.

Ditkof, J.N., 2013. Time-lapse seismic monitoring for enhanced oil recovery and carbon capture and storage field site at the Cranfield field, Mississippi. The University of Texas at Austin.

Duan, Z., Sun, R., 2003. An improved model calculating CO2 solubility in pure water and aqueous NaCl solutions from 273 to 533 K and from 0 to 2000 bar. Chem. Geol. 193, 257–271. https://doi.org/10.1016/S0009-2541(02)00263-2

Gassmann, F., 1951. Über die Elastizität poröser Medien. Vier. Der Natur 96, 1–23.

Gendrin, A., Fiah, N.M., Poupeau, F., Pekot, L.J., Garnett, A., 2013. Rewards and Challenges of Seismic Monitoring for CO2 Storage: A Fluid Substitution Study in the Gippsland Basin, Victoria, Australia. Energy Procedia 37, 4145–4154. https://doi.org/10.1016/j.egypro.2013.06.316

Hosseini, S.A., Lashgari, H., Choi, J.W., Nicot, J.-P., Lu, J., Hovorka, S.D., 2013. Static and dynamic reservoir modeling for geological CO2 sequestration at Cranfield, Mississippi, U.S.A. Int. J. Greenh. Gas Control 18, 449–462. https://doi.org/10.1016/j.ijggc.2012.11.009

Hovorka, S.D., Meckel, T.A., Treviño, R.H., 2013. Monitoring a large-volume injection at Cranfield, Mississippi—Project design and recommendations. Int. J. Greenh. Gas Control 18, 345–360. https://doi.org/10.1016/j.ijggc.2013.03.021

Ivanova, A., Kashubin, A., Juhojuntti, N., Kummerow, J., Henninges, J., Juhlin, C., Lüth, S., Ivandic, M., 2012. Monitoring and volumetric estimation of injected CO2 using 4D seismic, petrophysical data, core measurements and well logging: a case study at Ketzin, Germany. Geophys. Prospect. 60, 957–973. https://doi.org/10.1111/j.1365-2478.2012.01045.x

Kennett, B.L.N., 1983. Seismic wave propagation in stratified media, Cambridge University Press.

Kennett, B.L.N., 1974. Bulletin of the Seismological Society of America., Bulletin of the Seismological Society of America. The Society.

Lu, J., Kordi, M., Hovorka, S.D., Meckel, T.A., Christopher, C.A., 2013. Reservoir characterization and complications for trapping mechanisms at Cranfield CO2 injection site. Int. J. Greenh. Gas Control 18, 361–374. https://doi.org/10.1016/j.ijggc.2012.10.007

Marchesini, P., Ajo-Franklin, J. B., and Daley, T. M., 2017. In situ measurement of velocity-stress sensitivity using crosswell continuous active-source seismic monitoring, Geophysics, 82, D319-D326.

Mavko, G., Mukerji, T., Dvorkin, J., 2009. The rock physics handbook : tools for seismic analysis of porous media. Cambridge University Press.

Mukhopadhyay, S., Doughty, C., Bacon, D., Li, J., Wei, L., Yamamoto, H., Gasda, S., Hosseini, S.A., Nicot, J.-P., Birkholzer, J.T., 2015. The Sim-SEQ Project: Comparison of Selected Flow Models for the S-3 Site. Transp. Porous Media 108, 207–231. https://doi.org/10.1007/s11242-014-0361-0

Peng, D.-Y., Robinson, D.B., 1976. A New Two-Constant Equation of State. Ind. Eng. Chem., Fundam. 15, 59–64.

Roach, L.A.N., Angus, D.A., White, D.J., 2016. Assessment of the limitations on the seismic detectability of injected CO 2 within a deep geological reservoir. Energy Procedia. 13th Int. Conf. Greenh. Gas Control Technol. GHGT-13.

Smith, T.M., Sondergeld, C.H., Rai, C.S., 2003. Gassmann fluid substitutions: A tutorial. Geophysics 68.

Urosevic, M., Pevzner, R., Shulakova, V., Kepic, A., Caspari, E., Sharma, S., 2011. Seismic monitoring of CO2 injection into a depleted gas reservoir–Otway Basin Pilot Project, Australia. Energy Procedia 4, 3550–3557. https://doi.org/10.1016/j.egypro.2011.02.283

Vasco, D.W., Bakulin, A., Baek, H., Johnson, L.R., 2015. Reservoir characterization based upon the onset of time-lapse amplitude changes. GEOPHYSICS 80, M1–M14. https://doi.org/10.1190/geo2014-0076.1

Vasco, D.W., Daley, T.M., Bakulin, A., 2014. Utilizing the onset of time-lapse changes: a robust basis for reservoir monitoring and characterization. Geophys. J. Int. 197, 542–556. https://doi.org/10.1093/gji/ggt526

Weaver, L., Anderson, K., 1966. Cranfield field, Cranfield unit, Basal Tuscaloosa Reservoir, Adams and Franklin counties, Mississippi. Oil Recover. fromgas-cap Reserv. an Eng. Eval. Conserv. Pract. sixreservoirs. Interstate Oil Compact Comm. Oklahoma City 42–58.

Zhang, R., Sen, M.K., Srinivasan, S., 2014. Time-lapse pre-stack seismic inversion with thin bed resolution for CO2 sequestration from Cranfield, Mississippi. Int. J. Greenh. Gas Control 20, 223–229. https://doi.org/10.1016/j.ijggc.2013.10.032

Zhang, R., Song, X., Fomel, S., Sen, M.K., Srinivasan, S., 2013. Time-Lapse Seismic Registration and Inversion for CO_2 Sequestration Study at Cranfield Part II: Pre-Stack Analysis, in: SEG Annual Meeting. Society of Exploration Geophysicists, Houston, Texas.

Zhang, R., Song, X., Fomel, S., Sen, M.K., Srinivasan, S., 2012. Time-lapse surface seismic data registration and inversion for CO2 sequestration at Cranfield. Am. Geophys. Union, Fall Meet. 2012, Abstr. id. T12B-08.